Variability in Epithelial Backscattering via Dual-Mode Endomicroscopy for Early Cancer Detection

Remy Shea, Sylvia Lam, Michele Follen, Breana Hill, Varalee Chinsomboon, Magalie Tatischeff, Alan Harrison, CALUM MACAULAY

1 British Columbia Cancer Research Center Department of Integrative Oncology 675 West 10th Avenue, Vancouver BC, V5Z 1L3, Canada
2 Brookdale University Hospital and Medical Center, One Brookdale Plaza, Brooklyn NY, 11212, USA
*email: rshea@bccrc.ca

Summary

Early detection and treatment of oral precancers can drastically reduce the mortality rate of the disease. Previous work has demonstrated the ability of depth-dependent epithelial backscattering to resolve normal from dysplastic tissue in the oral cavity. We have developed an algorithmic approach to identifying sub-millimeter motion artifacts in the imaging probes field of view, in order to counteract a limitation of the imaging system. Further, classification thresholds have been identified which may lead to improvements in diagnostic sensitivity, accuracy and specificity for biopsy site selection, cancer screening and tumor margin assessment.

Introduction & Motivation

Dysplasia, a stage of pre-cancerous development in the epithelium is characterized into grades of severity mainly by the epithelial depth and degree to which nuclear clustering and enlargement in cell nuclei can be observed[1] (Figure 1).

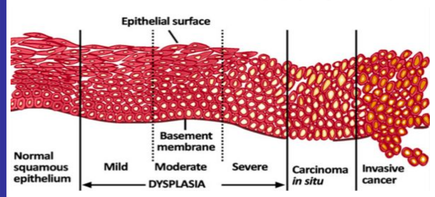

Figure 1. A illustration depicting the changes in cell density and nuclear enlargement associated with epithelial dysplasia in the course of it's progression to an invasive cancer.

A confocal dual-mode endomicroscopic setup was used to obtain synchronous, video-rate fluorescence endomicroscopy (FE) and diffuse optical microscopy (DOM) images from 6 anatomical sites (Figure 2) across 25 healthy volunteers of whom 12 were Male, 13 Female, ranging in age from 21 to 63. Images were also captured in 23 patients from the sites of their precancerous developments and a contralateral normal site.

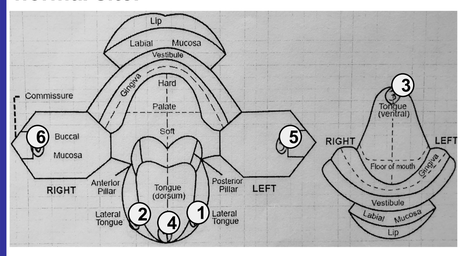

Figure 2. A diagram showing the 6 sites from which DME images were recorded in healthy volunteers. L-R Buccal Mucosa, Lateral Tongue, Dorsal and Ventral Tongue

Group	Patient (Train)	Volunteer Batch 2 (Train)	Volunteer Batch 2 (Test)
1 - Acceptable	7024	2354	2618
2 - Possibly Blurry	340	481	483
3 - Definitely Blurry	643	1413	1416
4 - Possibly Bad	37	939	941
5 - Definitely Bad	328	2578	2578
Total	8372	7765	7553

Table 1. Breakdown of DME fluorescence images by group membership. The dataset was manually annotated, with images sorted into groups, and later removed based upon reviewer consensus. In groups 1,3,4 and 5 reviewer consensus was above 95%.

Apparatus

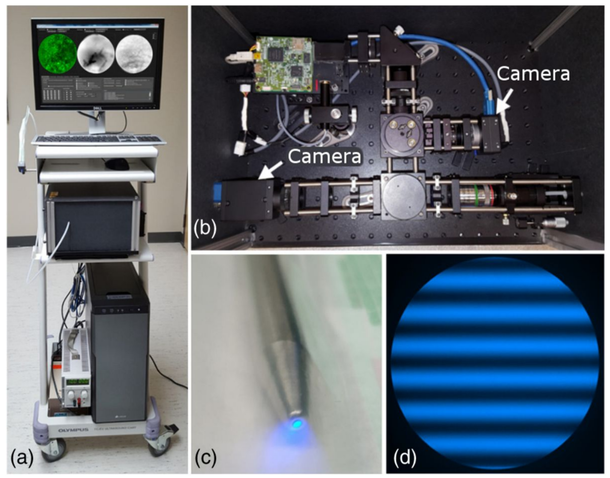

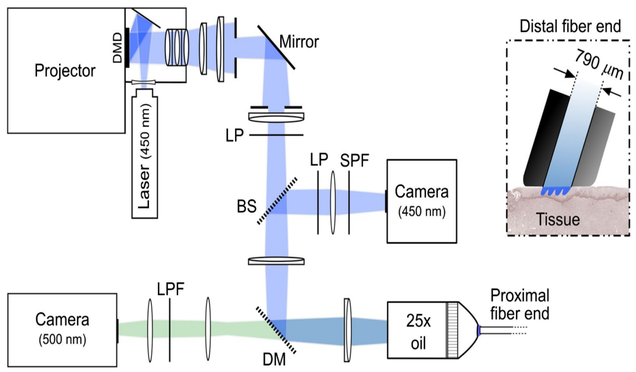

Figure 4. Schematic diagram of the DME setup combining FE and DOM to image both superficial microstructure and depth-dependent epithelial backscattering. The setup employs two digital cameras, a beam splitter and dichroic mirror to achieve separation of fluorescence and backscattering whilst the linear polarizer and filters purify signals.

Methods

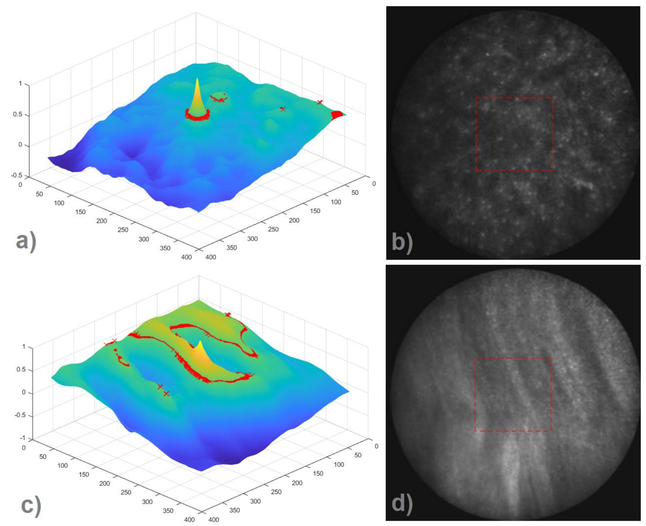

Figure 5. Depiction of the features used to characterize the auto-correlative surface of an image, generated by applying a 2-D cross correlation of the red boxes in 5.b) and 5.d) to the entire image. The red thresholds in 5.a) and 5.c) are the a contour of points with correlation of 0.4. The blurry image's autocorrelation surface has a higher proportion above this threshold.

A suite of features was created to identify motion in the DME probe's imaging field of view including image registration and power spectrum analysis features as well as texture and shape features from previous work.

We assume that a motionless image is relatively high contrast.The proportion of an image's autocorrelation surface above certain threshold values (0.4 shown in Figure[5]) were found to be useful metrics for identifying motion in the imaging probes field of view, with blurry images tending to have a greater area above the threshold. This is a result of the striations found in blurry images resembling themselves in the direction of the probe's movement.

The contrast-motion assumption is also reflected in the power spectrum of its 2D fast fourier transform. An exponential decay slope is fit to the power spectrum of an image, yielding a quantifiable measure of the image's blurriness (Figure [6]). A steeper slope typically indicates more motion, as smaller features on the scale of cellular structures cannot be resolved very well.

These features are used to classify images between acceptably still and unacceptable images. FE and DOM image acquisition is synchronous and so identifying still FE images means we can create a dataset comprised exclusively of still DOM images, counteracting the drawback of that modality alone.

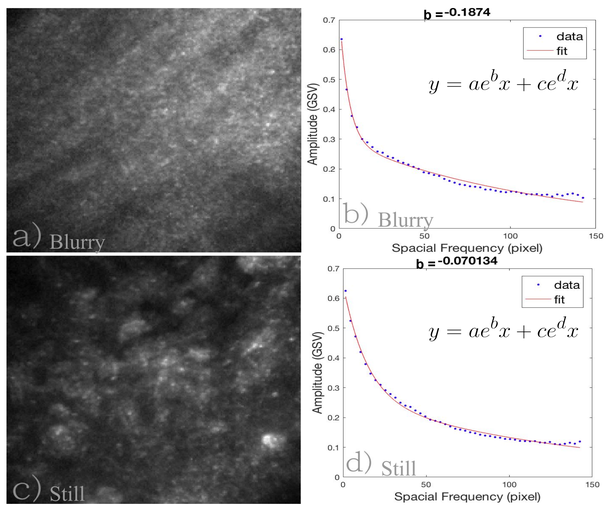

Figure 6. An illustration of the features extracted from power spectrum analysis of a subset of FE images, 6.a) & 6.c). The power spectra are fit to the equation shown in 6.b) & 6.d).

Results

Group	Training Dataset % (Total)	Test Dataset % (Total)
Acceptable	79.7 (9378)	75.1 (2618)
Non-Acceptable	89.6 (5938)	92.0 (4935)
Overall	83.4 (15316)	86.2 (7553)

Table 2. Performance of a binary tree in classifying DME fluorescence images. 'Non-Acceptable' includes groups 3,4,5 (group 2 was omitted as reviewer consensus was quite poor and could not agree on which groups these images belonged to, in addition, the size of the groups was small relative to the datasets).

A multivariate analysis of variance was then performed for each ratio of DOM backscattering signal across all identified still frames. We found that the inherent differences between subjects contributed the most to variance in the mean epithelial backscattering signal. The second most significant source of variance was the specific tissue site within the oral cavity where the image was gathered and finally we found that frames from the same video (considered repeat measurements of the same tissue) varied the least. We also found that the pattern of the ratios was consistent across tissue sites (Figure 4) and that the majority of ratios for the different sites were statistically different (except for Left Right differences in the same tissue type; sites 1-2 and 5-6).

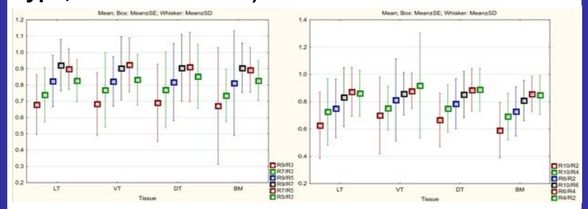

Figure 4. Ratios of the depth-dependent epithelial backscatter signal for different illumination spatial frequencies for the 4 oral tissue types; lateral tongue (LT), ventral tongue (VT), dorsal tongue (DT) & buccal mucosa (BM).

Conclusion

Our recent results strongly suggest that finding tissue site specific classifiers to identify transformed tissue (moderate - severe dysplasia or worse) will perform better than the global, organ specific classifiers developed so far. Following these results we are confident that a neural network trained upon the features we have developed and discussed here will perform better in classifying both image stillness and, separately, dysplasia and tissue abnormality than the histopathological gold standard screening. Ultimately, these advances may significantly improve the efficacy of screening and biopsy procedures.

Literature Cited & Acknowledgements

We acknowledge project funding by grants P01 CA82710 of the National Institutes of Health (NIH) and CPG-134740 of the Canadian Institutes of Health Research (CIHR). We strongly appreciate the participation of all patients and volunteers in this study. Personal thanks go to, Ian Janzen, Nico Bodenschatz, Kirk Madison and the dental assistants of the BC Cancer Agency Dental Clinic.

[1] S. Shirani, N. Kargahi, S. M. Razavi, and S. Homayoni, Iranian journal of medical sciences 39, 406 (2014).
[2] A.-B. Mosiciki, Y. Ma, C. Wibbelsman, T. M. Darragh, A. Powers, S. Farhat, and S. Shiboski, Obstetrics and gynecology 116, 1373 (2010).
[3] I. Abubakar, T. Tillmann, and A. Banerjee, Lancet 385,117 (2015).
[4] M. Contaldo, C. F. Poh, M. Guillaud, A. Lucchese,R. Rullo, S. Lam, R. Serpico, C. E. MacAulay, and P. M.Lane, Oral surgery, oral medicine, oral pathology and oral radiology 116, 752 (2013).
[5] N. Bodenschatz, S. F. Lam, A. Carraro, J. Korbelik, D. M. Miller, J. N. McAlpine, M. Lee, A. Kienle, and C. E. MacAulay, Journal of biomedical optics 21, 066001(2016).
[6] N. Bodenschatz, C. F. Poh, S. Lam, P. M. Lane, M. Guil laud, and C. E. MacAulay, Journal of biomedical optics 22, 086005 (2017)